GFZ
Helmholtz-Zentrum
POTSDAM

Originally published as:

Han, Y., Horsfield, B., Wirth, R., Mahlstedt, N., Bernard, S. (2017): Oil retention and porosity evolution in organic-rich shales. - *AAPG Bulletin*, *101*, 6, pp. 807—827.

DOI: http://doi.org/10.1306/09221616069

Oil retention and porosity evolution in organic rich shales

Yuanjia Han[1]*, Brian Horsfield[1], Richard Wirth[1], Nicolaj Mahlstedt[1], and Sylvain Bernard[2]

[1]German Research Centre for Geosciences (GFZ), Telegrafenberg, Potsdam 14473, Germany

[2]Institut de Minéralogie, de Physique des Matériaux et de Cosmochimie (IMPMC), Sorbonne Universités, CNRS UMR 7590, MNHN, UPMC, 61 rue Buffon, 75005 Paris, France.

ACKNOWLEDGEMENTS

This work was carried out in the framework of Yuanjia Han's Ph.D at the Technical University of Berlin, which was sponsored by the China Scholarship Council and Noble Energy. Special thanks are extended to Elke Lewerenz, Ilona Schäpan, and Anja Schreiber for their technical support.

ABSTRACT

Petroleum is retained in shales either in a sorbed state or in a free form within pores and fractures. In shales with oil resource potential, organic matter properties (i.e. richness, quality and thermal maturity) control oil retention in general. In gas shales, organic pores govern gas occurrence. While some pores may originate via secondary cracking reactions, it is still largely unclear as to how these pores originate. Here, we present case histories mainly for two classic shales, the Barnett Shale (Texas, USA) and the Posidonia Shale (Germany). In both cases, shale intervals enriched in free oil or bitumen are not necessarily associated with the layers richest in organic matter, but are instead associated with porous biogenic matrices. However, for the vast bulk of the shale, hydrocarbon retention and porosity evolution are strongly related to changes in kerogen density brought about by swelling and shrinkage as a function of thermal maturation. Secondary organic pores can form only after the maximum kerogen retention (swelling) ability is exceeded (at T_{max} around 445 ^{o}C, ~0.8%R_o). Shrinkage of kerogen itself leads to the formation of organic nano-pores, and associated porosity increase, in the gas window.

INTRODUCTION

The retention of hydrocarbons (HC) in shale is controlled mainly by the sorption capacity of its organic matter (Baker, 1962; Tissot et al., 1971; Stainforth and Reinders, 1990; Pepper, 1992), and a retention

threshold of 100 mg HC/g TOC (total organic carbon) has been proposed, irrespective of organic matter type and thermal maturity (Sandvik et al., 1992; Jarvie, 2012). Clay minerals, especially illite (Schettler and Parmely, 1991), have also been documented as possessing micropore structures capable of sorbing gas (Gasparik et al., 2012). In addition to sorption on particle surfaces, petroleum storage in the pores of either organic (Loucks et al., 2009) or inorganic (Han et al., 2015) origin have been documented, as well as natural fractures (Lopatin et al., 2003; Pollastro, 2010).

Organic pore development is believed to be largely due to the thermal cracking of kerogen (Jarvie et al., 2007; Loucks et al., 2009) and/or bitumen (Bernard et al., 2012b), though primary organic pores have been observed within immature organic matter as well (Löhr et al., 2015; Pommer and Milliken, 2015). The ability to predict the porosity evolution of shales as a function of thermal maturation is critical for successful well placement during the production of gas from shale resource plays, yet a comprehensive literature review reveals that the formation of secondary organic pores is only poorly understood.

Here we provide new insights into how oil retention and porosity evolution are related to changing kerogen density as a function of thermal maturation. The swelling of kerogen, directly linked to density change, was proposed as playing a role in petroleum fractionation and retention in organic-rich shales (Sandvik et al., 1992; Larsen and Li, 1997; Ertas et al., 2006; Kelemen et al., 2006a; Kelemen et al., 2006b). According to this theory, kerogen is believed to behave analogously to organic polymers, which are capable of absorbing significant quantities of oils by swelling. According to the model by Kelemen et al. (2006a), the bitumen retained in a given mass of Type-II kerogen first increases with increasing maturity until the maximum sorption capacity (209 mg/g TOC) is exceeded, and then declines. The first increase of bitumen in-place corresponds to the start of hydrocarbon generation in the early oil-window. With increasing maturity, the cracking and releasing of bulk labile hydrocarbon moieties from kerogen structures might most likely leave behind a more rigid and aromatic kerogen residue (Horsfield, 1989), accompanied by a decreasing ability for swelling (Ertas et al., 2006). Therefore, we can further deduce that the decrease of swelling ability is also accompanied by an increase in kerogen density (shrinkage), which is most likely brought about by bulk petroleum release, and then probably resulting in the formation of organic pores.

In the current study, and with central reference to the Posidonia Shale, a suite of techniques including Rock-Eval pyrolysis, mercury injection capillary pressure (MICP) porosimetry, focused ion beam (FIB)

combined with transmission electron microscopy (TEM) and scanning electron microscopy (SEM) were applied to study the relationship between oil retention and porosity evolution. Helium pycnometry was used to detect the density of isolated kerogen from Posidonia Shale (Rexer et al., 2014). Adding equivalent published data for the Barnett Shale (Hill et al., 2007b; Jarvie et al., 2007; Bernard et al., 2012b; Han et al., 2015; Reed and Loucks, 2015) a general model of oil retention and organic pore development has been built for these shales which contain Type-II organic matter with broadly similar structures (Behar and Jarvie, 2013).

MATERIALS AND METHODS

Samples

The Posidonia Shale is one of the most widespread and economically important source rocks of Western Europe (Littke et al., 1988). This Lower Toarcian age shale was deposited in an epicontinental sea under anoxic conditions (Röhl et al., 2001), spreading from the Yorkshire Basin (United Kingdom) over the Lower Saxony Basin (Germany) into the Paris Basin (France). Considered as a reference for Type-II kerogen of mainly algal origin (Rullkötter and Marzi, 1988), the Posidonia Shale is rich in organic matter and coccolith-derived carbonate (Littke et al., 1988; Röhl et al., 2001).

This study reports on data for six boreholes penetrating the Posidonia Shale, namely Wenzen (WEN), Wickensen (WIC), Dielmissen (DIE), Dohnsen (DOH), Harderode (HAR) and Haddessen (HAD), drilled in the Hils Syncline of the Lower Saxony Basin, northern Germany (Figure 1A). These six wells represent a maturity sequence from 0.48 to 1.45% R_o (Jochum et al., 1995; Bernard et al., 2013), with only minor variations in organic geochemical composition and mineralogy (Littke et al., 1988; Rullkötter and Marzi, 1988), although the maturation history has been a matter of dispute (Gasparik et al., 2014). Here we base the interpretation of our results on the assumption that the organic matter was never deeply buried (<1800 m; Figure 1B) but thermally altered by a deep seated igneous intrusion (Littke et al., 1988; Düppenbecker, 1992; Jochum et al., 1995; Gasparik et al., 2014), the Vlotho Massif, of Turonian age (93.6-88.6 Ma). Thus, the compaction of the Posidonia Shale has not proceeded since that time.

The Mississippian Barnett Shale is one of the most well-known shale gas plays in the United States (Jarvie et al., 2007). In the Fort Worth Basin, this black shale was deposited in a deep ocean under anoxic conditions with primary productivity being enhanced by upwelling (Loucks and Ruppel, 2007). The organic-rich Barnett

Shale is a typical marine source rock, with abundant biogenic-derived quartz (Bowker, 2003; Loucks and Ruppel, 2007; Milliken et al., 2007; Han et al., 2015). Three Barnett Shale samples from the Marathon 1 Mesquite well (Han et al., 2015) are used to compare to the Posidonia Shale. These Barnett Shale samples have late oil window maturity (1.02% R_c). Two thin sections were selected from the siliceous 2nd interval to target the sponge spicules, and the other bulk core sample was taken from the argillaceous 3rd interval for FIB foil extraction.

Rock-Eval pyrolysis and Total Organic Carbon (TOC) determination

Rock-Eval pyrolysis (Espitalie et al., 1977) was performed on 476 whole-rock Posidonia Shale samples using a Rock-Eval 2 instrument. For TOC analysis, a Leco SC-632 combustion oven (1350 °C in oxygen for oxidation) was used with IR (infra-red) detection, after treating finely crushed rock samples with HCl (1:9 HCl:Water) at 60 ±5 °C to remove carbonate.

Mercury Injection Capillary Pressure Porosimetry and Helium Pycnometry

The porosity measurements were carried out using mercury injection capillary pressure (MICP) porosimetry and helium pycnometry as described in detail in Rexer et al. (2014). Data collected from the literature (Gasparik et al., 2014; Rexer et al., 2014) are reported together with newly acquired data for Posidonia Shale samples in Table 1.

Focused ion beam (FIB) combined with TEM and SEM

Preparation of focused ion beam (FIB) foils for 15 Posidonia Shale and three Barnett Shale samples follows the procedure described in Wirth (2009). TEM was performed in a TECNAi F20 X-Twin transmission electron microscope with a field emission gun electron source. The TEM was operated at 200 keV, with a nominal camera length of 330 mm. TEM images were acquired as high-angle annular dark-field images (HAADF) in Z-contrast mode or as energy –filtered images applying a 200 keV window to the zero-loss peak. Energy-dispersive X-ray spectroscopy (EDXS) analysis was carried out using an EDXS X-ray analyser with ultra-thin window. Most foils are extracted from cores directly, but two foils are extracted from thin sections to target porous fossils (sponge spicules). Scanning electron microscopy (SEM) was performed in the way described in Bernard et al. (2013).

RESULTS AND DISCUSSION

Oil Retention

The total amount of oil retained in a given shale can be quantified using Rock-Eval data from original and solvent extracted rocks (Jarvie, 2012; Han et al., 2015):

$$\text{Total-oil} = S1_{\text{whole rock}} + S2_{\text{whole rock}} - S2_{\text{extracted rock}}$$

S1 corresponds to the yield of thermally extractable hydrocarbons present in the rock that are volatilized at nominal temperatures at or below 300 °C, which is about 40 °C lower than the true temperature in the oven when using Rock-Eval 2 instrument. S2 is the yield of pyrolysis products generated at a temperature up to 650 °C. Because the calculated amount of total-oil and the S1 value of unextracted rocks are strongly correlated (Han et al., 2015), S1 has been used in the ensuing discussions as a proxy for the retained oil concentration. Note that the proportion of S1 to total-oil may vary depending on the maturity level.

In accordance with previous studies (Tissot et al., 1971; Pepper, 1992; Sandvik et al., 1992; Han et al., 2015), the retention of oil in the Posidonia Shale is shown to be controlled primarily by organic matter richness (Figure 2). For a given well, e.g. the immature Wenzen well (blue diamonds, WEN 0.48% R_o), a linear trend between organic richness (TOC) and the amount of in place hydrocarbons (S1) indicates that most oil is retained in a sorbed state on the organic matter. But exceptions exist, for example some samples in the Wickensen well (red squares, WIC 0.53% R_o) exhibit higher S1 values than expected from its specific linear trend (Figure 2). S1 values encountered for those samples exceed TOC contents nominally, a feature called "oil crossover" corresponding to oil saturation index values (OSI = [S1/TOC] × 100) higher than 100 mg HC/g TOC (Jarvie, 2012).

Transmission electron microscopy (TEM) has revealed that oil crossovers occur in the Posidonia Shale where calcareous coccoliths are abundant (Figure 3A). A similar retention phenomenon related to the presence of porous fossils exists in the Marathon 1 Mesquite well (Han et al., 2015), where siliceous sponge spicules enhance the storage capacity for bitumen (Figure 3B). Hence, those porous fossiliferous shale layers, though less common, constitute sweet spots as they exhibit enhanced hydrocarbon potentials. Oils are stored in a free state within the matrix porosity and thus should be easier to be produced. The higher carbonate/silica content of these layers also implies a more brittle behavior.

Except for these fossiliferous layers, oil retention in the Posidonia shale is clearly dominated by sorption of the organic matter (Figure 2), which is affected by thermal maturation as follows. For the vast bulk of Posidonia samples (Figure 2), the slope of the trend-line first increases above that of the immature Wenzen well (blue diamonds, WEN 0.48% R_o) to that of oil-mature Dielmissen well (green triangles, DIE 0.68% R_o), and then subsequently decreases with increasing maturity to that of the gas-mature Haddessen well (yellow circles, HAD 1.45% R_o). A first increase and then decrease of oil retention capacity is shown.

In Figure 4, the averaged OSI values are used to represent the oil retention capacity for a given amount of kerogen in each Posidonia well, and are plotted together with published data from the Barnett Shale in the same maturity context (T_{max}). It can be readily seen that the TOC normalized retention capacity (OSI) of the Posidonia and Barnett shales follows the same evolution pathway (Figure 4). With increasing maturity, the OSI values gradually increase until a maximum retention capacity about 90 mg S1/g TOC is reached at T_{max} values around 445 ºC, and then a subsequent decrease is shown. It should be noted here that the "true" maximum oil retention capacity, in terms of retained total-oil following the empirical formula [Total-oil = 2.1556 × S1] given in figure 8-C in Han et al. (2015), is about 195 mg total-oil/g TOC.

Here we draw attention to the fact that a qualitatively and quantitatively very similar retention pathway is predicted by kerogen swelling theory (Kelemen et al., 2006a) with a theoretically predicted range of 161 to 209 mg bitumen/g C_{org} for Type-II organic matter. That changing oil retention capacity evolves with increasing maturity in the same manner as that of the Posidonia and Barnett Shales (Figure 4), as well as of the Toarcian Shale in the Paris Basin where 200mg total oil/g TOC was reported (Tissot et al., 1971). A logical conclusion is that the oil retention capacity of shale is governed by the swelling behaviour of the kerogen as a function of maturity. The first increase of oil in-place may correspond to the generation of hydrocarbon in early oil-window. But with increasing maturity, the thermal cracking and releasing of labile hydrocarbon moieties from kerogen rise to a maximum at a T_{max} of about 445 ºC, which most likely will leave behind a more rigid kerogen residue. Subsequently, the swelling ability of kerogen network correspondently decreases. In support of this hypothesis, we note here that the reported density increase of Type-II kerogen at T_{max} of 440-450 ºC (Okiongbo et al., 2005) is concomitant with the decrease of oil concentration (per gram organic carbon) in shales at T_{max} values around 445 ºC (Figure 4).

Extending that concept, it can be deduced that the lower the degree of swelling, the higher the density of the kerogen. For the Posidonia Shale, the density of isolated kerogen (Rexer et al., 2014) follows the order: Haddessen (1.368-1.342 g/cm^3) > Wickensen (1.235-1.217 g/cm^3) > Harderode (1.168-1.024 g/cm^3). Retained oil concentrations behave exactly the other way around (Haddessen [21 mg/g TOC] < Wickensen [36 mg/g TOC] < Harderode [53 mg/g TOC], Table 2). Therefore, retained oil concentrations are inversely proportional to kerogen density and reflect the degree of kerogen swelling.

One interesting consequence of this relationship is that individual kerogen components or macerals may exhibit different retention capacities. For instance, the measured inertinite density (1.40 g/cm^3) (Robl et al., 1987) is obviously higher than that of other macerals (alginite 1.01 g/cm^3, bituminite 1.16 g/cm^3, vitrinite 1.25 g/cm^3). Thus, a weaker sorption/swelling ability can be inferred for inertinite, which might explain the weaker sorption control of inert over labile kerogen (Han et al., 2015). Nevertheless, it should be noted that inert kerogen is not necessarily identical to inertinite but, as opposed to labile kerogen, represents only the fraction of kerogen which does not generate petroleum (Cooles et al., 1986).

Overall, it is the organic matter properties, i.e. richness, composition and thermal maturity that control the oil retention in general. In organic-rich shales, the retention of oil is primarily controlled by the TOC content, in which the inert kerogen possesses a weaker sorption control than the labile kerogen. With increasing maturity, the TOC normalized concentration of retained oil (S1/TOC×100) first increases in the oil window, until the maximum retention ability (about 90 mg HC/g TOC) is exceeded at T_{max} around 445 °C. Afterwards, due to a reduction in the kerogen retention/swelling ability brought about by an increase in kerogen density most likely caused by the thermal cracking of labile precursor structures leaving behind a more rigid and aromatic kerogen residue (Horsfield, 1989), the TOC normalized concentration of retained oil (S1/TOC×100) shows a subsequent decrease.

Porosity Evolution

The Posidonia Shale's porosity evolves with increasing maturation (Figure 5), from 5-17% for immature Wickensen samples to 1-6% for oil-mature Harderode samples to 6-17% for overmature Haddessen samples. A similar evolution trend of porosity has also been reported for the New Albany Shale (Mastalerz et al., 2013). Such evolution differs from a classic porosity-depth relationship, that is, a simple exponential decrease with increasing depth/maturity (Hedberg, 1936; Sclater and Christie, 1980; Tissot and Welte, 1984). In accordance

with recent studies on organic pores (Loucks et al., 2009; Curtis et al., 2011; Bernard et al., 2012a; Bernard et al., 2012b; Curtis et al., 2012; Pommer and Milliken, 2015), we presume that the latter increase of porosity is, to a large extent, reflecting the formation of organic pores as the thermal conversion of organic matter takes place (Jarvie et al., 2007).

To examine this hypothesis qualitatively, FIB-TEM analysis was conducted on a maturity suite of Posidonia Shale foils. There were no visible pores detected within organic matter of the Wickensen (427 °C T_{max}, Figure 6A) and Harderode (446 °C T_{max}, Figure 6B) wells. But as maturity increases, the isolated bubble-like pores start to occur within the organic matter of the Dohnsen well (449 °C T_{max}, Figure 6C), and become much more significant with a sponge-like appearance in the Haddessen well (458 °C T_{max}, Figure 6D). The formation of secondary organic pores in the Posidonia Shale initiates at the maturity range of 446-449 °C T_{max}, which may therefore contribute to the latter increase of porosity in the Posidonia Shale (Figure 5).

To further demonstrate the above hypothesis quantitatively, the volume change of organic matter with increasing maturity is here calculated for the Posidonia Shale (Table 2). Kerogen density obtained through helium pycnometry (Rexer et al., 2014) allows TOC masses to be converted into organic matter volumes. Surprisingly, the volume of organic matter in the immature Wickensen well (21.07 vol.%) is nearly the same as in the oil-mature Harderode well (20.84 vol.%), even though their corresponding TOC values vary significantly (10.41 wt.% versus 7.90 wt.%). In other words, the density of organic matter has decreased from 1.226 to 1.096 g/cm^3 (Table 2). This observation differs from the classic assumption (Ungerer et al., 1983) that the density of Type-II kerogen increase continuously with increasing maturity. It is worth noting that the uncertainty over whether the density was based on extracted kerogen may account for this discrepancy.

Nevertheless, the decrease in kerogen density [0.130 g/cm^3, Equation (1)] contributes only a portion [1.10 wt.%, Equation (2)] of the TOC difference [2.51 wt.%, Equation (3)] between the Wickensen and Harderode wells (Table 2). The rest can be tracked back to dilution mainly by mineral cementation, which also resulted in the reduction of Posidonia Shale porosity in the oil window (Figure 5). The diagenetic cementation of pyrite (Figure 7), quartz (Figure 8), and calcite (Figure 8) are commonly observed in the mature Harderode and Haddessen wells, but only to a lesser extent in the immature Wickensen well (Bernard et al., 2013). Accordingly and probably due to a combination of cementation and additional dilution through terrestrial input, the volume of mineral matrix in the Harderode (75.12 vol.%) and Haddessen (74.37 vol.%) wells is

about 10 vol.% higher than that in the Wickensen well (64.90 vol.%) in Table 2. The TOC content must then be diluted relatively by minerals [1.24 wt.%, Equation (4)]. Meanwhile, the high porosity seen in the immature Wickensen well (14.03 vol.%) has been reduced by roughly 10 vol.% to 4.05 vol.% in the oil-mature Harderode well. Cementation rather than compaction is responsible for the decrease of oil-mature Harderode sample porosity. Those results are in line with the hypothesis that the studied wells have never been deeply buried (<1800m; Figure 1B) and that compaction of Posidonia Shale in the Hils Syncline area has not proceeded since the initiation of thermal maturation by the deep seated igneous intrusion, Vlotho Massif (Düppenbecker, 1992).

Given that lateral facies variations between the studied Posidonia wells are only minor (Littke et al., 1988; Rullkötter and Marzi, 1988), the oil-mature Harderode well is treated as the less mature precursor of the gas-mature Haddessen well. It is believed that secondary nanoporosity arises in the organic matter (OM) as a result of thermal conversion (Jarvie et al., 2007; Loucks et al., 2009). In the case of negligible compaction, secondary organic porosity can be calculated by comparing the volume change of kerogen. As the kerogen volume of Haddessen well is 13.50 vol.% (Table 2) and that of Harderode well is 20.84 vol.%, a net 7.34 vol.% of secondary organic pores ought to been formed. Thus, 35% of the volume of organic matter in the Harderode well [7.34/20.84×100% = 35%, Equation (5)] should be converted into organic pores in the Haddessen well. Under SEM, OM-hosted porosity shows significant heterogeneity among the different kerogen particles in the Haddessen well (Figure 9). SEM distinguishable porosity is estimated to fall in the 10% to 30% range relative to the host particles. Considering that nanopores developed within the bitumen/pyrobitumen as well (Bernard et al., 2012b), and those bitumens can be extremely porous (>50% bitumen volume; Figure 8), we conclude that 35% OM-hosted porosity is generated within the gas-mature organic matter, and these thermally derived secondary organic pores (7.34 vol.%) contribute a large fraction of the porosity increase [8.08 vol.%, Equation (6)] observed between the Harderode and Haddessen maturity stage (Figure 5).

To summarise the results above, it is mainly cementation that reduced the porosity from 14.03 vol.% in the immature Wickensen Well to 4.05 vol.% in the oil-mature Harderode Well. The compaction of Posidonia Shale in the Hils Syncline area has not proceeded since the initiation of thermal maturation. Correspondently, the latest formed organic pores were not compacted, and therefore can bring about 7.34 vol.% porosity

increase in the gas-mature Haddessen Well. In line with previous studies, the formation of organic pores due to thermal conversion of kerogen is demonstrated, and here initiates at the maturity range of 446-449 °C T_{max}.

In the investigated Posidonia Shale, a discrepancy in estimated maturity exists between T_{max} and R_o values, something which has been reported previously (Price and Baker, 1985; Peters, 1986). The average T_{max} value of Dohnsen well is about 449 °C (Figure 4), which is higher than that of Harderode well (446 °C T_{max}). But the measured vitrinite reflectance of Dohnsen well (0.73% R_o, Figure 10) is otherwise lower than that of Harderode well (0.85% R_o). Considering that the T_{max} values applied here are the average of more than 48 samples for each well, these are statistically meaningful when it comes to signalling maturity. Vitrinite reflectance, on the other hand, has to be determined on vitrinite particles which are not abundant in the case of Type-II kerogens. Differences in vitrinite reflectance interpretation for the Harderode well have been published (Littke et al., 1988; Rullkötter and Marzi, 1988). In balance, we have concluded that the formation of organic pores in the Posidonia Shale begins in the maturity range 446-449 °C T_{max} or 0.73-0.85% R_o.

The appearance of secondary organic pores in the Barnett Shale is reported as being at 0.85% R_o, as compiled in Table 3. Other shales that span immature to overmature levels, show the occurrence of secondary organic pores at 0.75% R_o (Avalon Shale), at 0.75% R_o (Eagle Ford Formation), at 1.23% R_o (Woodford Shale), and at 0.78% R_o (a combination of the Marcellus, New Albany and Pearsall shale units) (Table 4). A key piece of information retrieved from these data packages (Table 3 and Table 4) is that the development of secondary organic pores seems to start at or around a maturity of 0.8% R_o.

If we envisage that the observed secondary organic pore space was originally occluded by oil/bitumen, the presence of those pores can be treated then as a tracer of nascent or ongoing petroleum expulsion. It is noteworthy that, according to the assessment of 253 crude oils from worldwide petroleum systems (Radke, 1988), the most common maturity of Type-II crude oils is centred around 0.8% R_o. This coincides with the maturity level for the appearance of organic pores in the Posidonia, Barnett, and other shales. As previously discussed, the swelling capacity of Type-II kerogen is decreasing at T_{max} around 445 °C (Figure 4), which is equal to about 0.8% R_o as well (Figure 10). For Type-I kerogen, oil generation was believed to occur within a narrow T_{max} range of 440-450 °C (Tissot et al., 1987), and peak expulsion was reported to initiate in a relatively low maturity level of 0.65-0.75 %R_c (Radke, 1988). For Type-III kerogen, a higher maturity level

(>450 ºC T_{max},0.82-0.90 %R_c) seems to be requested for bulk generation (Tissot et al., 1987) and expulsion (Radke, 1988).

Gas Loss

Due to evaporative gas loss during sample storage and handling, C_1 to C_5 gas components are mainly depleted in core samples (Larter, 1988; Sandvik et al., 1992). Even though the gas loss (Price et al., 1983; Larter, 1988; Sandvik et al., 1992) can be conceived as a contributor in shaping the OSI curves, such as that we have presented here (Figure 4 and Figure 10), it is important to note that the decrease in retained oil is not derived by gas loss. To examine the role of gas loss, we have examined methane sorption data (Gasparik et al., 2014). The maximum excess sorbed methane measured (65 ºC, 25MPa) on dry samples of the individual Posidonia wells is 13 mg CH_4/g TOC for Wickensen (0.53% R_o), 14 mg CH_4/g TOC for Harderode (0.85% R_o) and 22 mg CH_4/g TOC for Haddessen (1.45% R_o). After adding this methane potential to the corresponding OSI values, the arch-like formed trend still remains (Figure 4). In addition, this methane potential can be viewed as a maximum methane potential because gas sorption capacity is reduced by 40 to 60% for pristine (freshly taken) compared to dry samples (Gasparik et al., 2014). Thus, decreasing OSI values for T_{max} exceeding 445ºC (~0.8% R_o) are not due to gas loss. In fact, the evolution of oil retention capacity/threshold shows an inflexion at a maturity level that is obviously lower than that of significant gas generation. For the Posidonia Shale, the secondary cracking of oil into gas was reported to start around 1.2% R_o (Dieckmann et al., 1998), whereas for the Barnett Shale, the start of significant gas generation is reported to occur at a maturity higher than 1.1% R_o (Jarvie et al., 2005; Hill et al., 2007a).

Volumetric Calculation of Organic Matter

Previously, a constant value of 1.2 was used for the conversion of TOC (wt.%) into kerogen mass (Table 2). But we recognize that the content of carbon in total organic matter increases with increasing maturity (Baskin and Peters, 1992b) as well. If 76 wt.%, 88 wt.% and 90 wt.% of the carbon content in kerogen given by Ungerer et al. (1983) is assumed for the Wickensen (0.53% R_o), Harderode (0.85% R_o) and Haddessen (1.45% R_o) wells, the recalculated kerogen volumes are 23.10 vol.%, 19.73 vol.% and 12.50 vol.% respectively. Organic porosity expected to be formed by kerogen shrinkage [19.73 – 12.50 = 7.23 vol.%, Equation (7)] is almost identical to our previous result (7.34 vol.%).

Compaction of Organic Pores

Notably, some deviations from the above interpreted trend of organic pore development can be gleaned from the literature. For example, pores have been reported in immature organic matter of the Eagle Ford Formation (Pommer and Milliken, 2015), probably inherited from precursor biomass (Table 4). This kind of primary organic pores is also observed in the immature Posidonia Shale (Figure 11A). Different from the secondary organic nanopores, the primary micrometre-size organic pores detected here have regular walls and an elongated shape that is aligned with the host particle.

Besides that, some gas mature shales exhibit an absence or paucity of OM-hosted pores (Table 4), ostensibly because of compaction after or synchronous to their formation (Curtis et al., 2012). As exemplified in the Marathon 1 Mesquite well (1.02% R_o), no visible pores were developed within organic matter showing features of compaction (Figure 11B), while they are sometimes abundant in organic matter of possible bitumen origin (Figure 11C). In the latter cases organic matter is potentially protected by surrounding rigid grains, one example being the organic matter stored in the chamber of sponge spicules (Figure 11D). This may further explain the preferential sheltering of pores in areas between, within, and around rigid grains (Pommer and Milliken, 2015), i.e. in the pressure shadows.

CONCLUSION AND IMPLICATIONS

Oil retained in shales is present either in a sorbed state or in a free form within pores and fractures. Organic matter properties, i.e. richness, composition and thermal maturity control oil retention in general. In the bulk volume of the Posidonia and Barnett Shales, the retention of oil is primarily controlled by the organic richness (TOC), in which the inert kerogen possesses a weaker sorption control than does the labile kerogen. With increasing maturity, the TOC normalized concentration of retained oil (S1/TOC×100) increases in the oil window, until the maximum retention ability (90 mg HC/g TOC) is exceeded for these kerogens at T_{max} around 445 °C (~0.8% R_o). The oil retention capacity is hereby governed by kerogen swelling. The cracking and releasing of bulk labile hydrocarbon moieties from kerogen structures at vitrinite reflectance about 0.8% R_o most likely leaving behind a more rigid kerogen residue, and then the swelling/retention ability of kerogen network is decreased subsequently. Interestingly, shale intervals enriched in normalised oil or bitumen yield are not necessarily associated with the organic richest layers, but rather to porous biogenic matrices.

We believe that our observations and synthesis with key literature are consistent with organic pores being formed by the shrinkage of kerogen, beginning for Type-II source rocks at around 0.8% R_o. Since the shrinkage is tracked by a significant density increase which otherwise reflects the decrease of kerogen swelling ability, the point where oil retention capacity starts to decrease (445 ^oC T_{max} or 0.8% R_o) is therefore expected to reflect the start of organic nanopores to occur. Notably, newly formed organic pores may be closed again by compaction. Given the remarkable heterogeneity in shale fabric, some deviations from the above trend may be due to local differences in compaction.

Table 1. Porosity and density data of three Posidonia wells.

Sample	Well	Depth	Maturity	TOC	Hg_Density	Hg	He	Bulk	Kerogen
		(m)	Ro (%)	(wt.%)	(g/cm³)	Porosity (vol.%)		He_Density (g/cm³)	
G007129	Wickensen	30.2	0.53	11.40		9.84			
G007133	Wickensen	34.1	0.53	8.40		12.76			
G007135	Wickensen	36.1	0.53	12.70		10.05			
G007137	Wickensen	38.8	0.53	10.30		10.61			
G007139	Wickensen	40.2	0.53	9.38		13.52			
G007142	Wickensen	43.6	0.53	10.20		12.02			
G007143[G]	Wickensen		0.5	14.10				2.249	
G007145	Wickensen	47.4	0.53	9.97		12.85			
G007145[R]	Wickensen	47.4	0.53	10.92	1/0.497		13.80	2.321	1.217
G007147	Wickensen	49.8	0.53	7.84		5.37			
G007149[G]	Wickensen		0.5	11.70				2.313	
G007151	Wickensen	53.1	0.53	8.90		10.22			
G007152	Wickensen	54.6	0.53	11.40		15.40	16.60	2.337	
G007153	Wickensen	55.7	0.53	7.59		13.87			
G007155	Wickensen	57.8	0.53	11.40		12.63			
G007155[R]	Wickensen	57.8	0.53	9.67	1/0.484		12.50	2.297	1.235
G007156	Wickensen	58.2	0.53	9.86			13.23	2.658	
G007156[G]	Wickensen		0.5	11.70				2.658	
Average				10.41	2.039	11.60	14.03	2.405	1.226
G007038	Harderode	44.5	0.85	7.90		1.30	3.32	2.490	
G007038[G]	Harderode		0.9	9.30				2.488	
G007038[R]	Harderode	44.5	0.89	7.91	1/0.414		3.10	2.468	1.168
G007046	Harderode	52.0	0.85	6.67			4.46	2.502	
G007060	Harderode	66.8	0.85	5.87		4.47	5.35	2.560	
G007060[G]	Harderode		0.9	6.80				2.559	
G007060[R]	Harderode	66.8	0.89	5.78	1/0.404		4.50	2.550	1.024
G007070	Harderode	76.1	0.85	9.97		3.51	3.55	2.488	
G007070[G]	Harderode		0.9	10.90				2.488	
Average				7.90	2.445	3.09	4.05	2.510	1.096
G007083	Haddessen	35.1	1.45	6.80		13.67			
G007090	Haddessen	40.1	1.45	7.70		11.23			
G007090[R]	Haddessen	40.1	1.45	7.41	1/0.439		11.40	2.556	1.342
G007094	Haddessen	44.1	1.45	5.08		12.01			
G007097	Haddessen	45.6	1.45	6.20		11.87			
G007099	Haddessen	47.7	1.45	6.59		10.60			
G007101a	Haddessen	49.6	1.45	5.37		11.77			
G007101b	Haddessen	49.6	1.45	5.37		10.92			
G007103	Haddessen	50.8	1.45	5.64		6.75	8.26	2.595	
G007103[G]	Haddessen		1.5	6.70				2.595	
G007104	Haddessen	51.1	1.45	5.04		11.63			
G007105	Haddessen	51.7	1.45	5.54		11.23			
G007110	Haddessen	55.7	1.45	6.12		9.36			
G007115	Haddessen	58.1	1.45	5.39		9.30	8.53	2.580	
G007115[G]	Haddessen		1.5	7.70				2.580	
G007119	Haddessen	60.6	1.45	7.71		11.28	14.64	2.610	
G007119[G]	Haddessen		1.5	7.70				2.608	
G007119[R]	Haddessen	60.6	1.45	7.15	1/0.445		13.70	2.614	1.368
G007123	Haddessen	63.8	1.45	8.29			16.27	2.470	
G007123[G]	Haddessen		1.5	10.50				2.470	
G007127	Haddessen	65.1	1.45	7.83		7.02			
Average				6.75	2.263	10.62	12.13	2.568	1.355

Data collected from Gasparik et al. (2014) and Rexer et al. (2014) are superscripted with G and R, respectively.

Table 2. Averaged values for a variety of discussed key parameters in three Posidonia wells.

Posidonia	Maturity		TOC‡	OSI$	Kerogen‡	Shale‡	Pore‡	Kerogen*	Mineral*	Shale*	Mineral*
Well	Ro (%)†	T_{max} (°C)$	(wt.%)	(mg/gTOC)	(g/cm³)	(g/cm³)	(vol.%)			(g/cm³)	(g/cm³)
Wickensen	0.53	426.72	10.41	36	1.226	2.039	14.03	21.07	64.90	2.067	2.787
Harderode	0.85	445.69	7.90	53	1.096	2.445	4.05	20.84	75.12	2.409	2.903
Haddessen	1.45	457.61	6.75	21	1.355	2.263	12.13	13.50	74.37	2.256	2.788

†Vitrinite reflectance are taken from Bernard et al. (2012a), ‡TOC, ‡density and ‡porosity values are averages from Table 1, $$T_{max}$ and $OSI values are averaged from our data base, computed data are marked with asterisk*. The accuracy of calculation can be evaluated by comparing computed and measured shale density data. By multiplying a constant of 1.2 (assuming 83 wt.% of carbon in organic matter), the total organic matter masses were calculated from the TOC. Although we recognize that the content of carbon in total organic matter increases with increasing maturity (Baskin and Peters, 1992a), a constant of value (83 wt.%) is here assumed, but it is discussed in detail in the discussion chapter.

Table 3. The data package collected (Loucks et al., 2009; Wang et al., 2009; Milner et al., 2010; Passey et al., 2010; Bernard et al., 2012b; Gareth R. Chalmers et al., 2012; Robert G. Loucks et al., 2012; Loucks and Reed, 2014; Reed et al., 2014) for the Barnett Shale to illustrate the occurrence of organic pores with increasing maturity.

Literature	Shale	Authors' Figure	R_o (%)	T_{max} (°C)	R_c (%)	Organic Pore	Note
Bernard et al., 2012	Barnett	Figure 4		420	0.40	No	
Loucks et al., 2009	Barnett	Figure 10-A	<0.5			No	
Loucks et al., 2012	Barnett	Figure 11-C	0.5			No	
Loucks &Reed, 2014	Barnett	Figure 3-C	0.51			No	
Loucks et al., 2009	Barnett	Figure 10-B	0.52			No	
Reed et al., 2014	Barnett	Figure 1-A	0.85			Yes	Bubble-like
Reed et al., 2014	Barnett	Figure 1-B	0.91			Yes	Elongate
Reed et al., 2014	Barnett	Figure 1-D	0.91			Yes	Bubble-like
Loucks &Reed, 2014	Barnett	Figure 5-A/B	1.25			Yes	Sponge-like
Loucks et al., 2012	Barnett	Figure 10-F	1.31			Yes	Sponge-like
Loucks et al., 2012	Barnett	Figure 10-E	1.35			Yes	Sponge-like
Loucks et al., 2012	Barnett	Figure 13-A	1.35			Yes	Sponge-like
Loucks et al., 2009	Barnett	Figure 5-A/B	1.35			Yes	Sponge-like
Loucks et al., 2009	Barnett	Figure 6	1.35			Yes	Bubble&Sponge
Milner et al., 2010	Barnett	Figure 5-A/B	1.5			Yes	/
Reed et al., 2014	Barnett	Figure 2		482	1.55	Yes	Sponge-like
Loucks et al., 2012	Barnett	Figure 10-A	1.6			Yes	Sponge-like
Loucks et al., 2012	Barnett	Figure 10-B	1.6			Yes	Sponge-like
Loucks et al., 2012	Barnett	Figure 11-A	1.6			Yes	Sponge-like
Loucks et al., 2009	Barnett	Figure 5-C	1.6			Yes	Elongate
Loucks et al., 2009	Barnett	Figure 5-D	1.6			Yes	Uncommon
Wang et al., 2009	Barnett	Figure 1	1.6			Yes	Bubble&Sponge
Passey et al., 2010	Barnett	Figure 27	1.8			Yes	Sponge-like
Bernard et al., 2012	Barnett	Figure 6		>500	>1.84	Yes	Sponge-like
Milliken et al., 2012	Barnett	Figure 7	1.5-2.0			Yes	Sponge-like
Loucks &Reed, 2014	Barnett	Figure 5-C	1.9-2.2			Yes	Sponge-like
Chalmers et al., 2012	Barnett	Figure 11	2.25			Yes	Elongate &Sponge
Loucks et al., 2012	Barnett	Figure 11-B	3.17			Yes	Sponge-like

T_{max} values were converted to equivalent R_c (%) by applying equation: $R_c = 0.018 \times T_{max} - 7.16$ (Jarvie et al., 2007).

Table 4. The data package collected (Milner et al., 2010; Schieber, 2010; Curtis et al., 2011; Curtis et al., 2012; Gareth R. Chalmers et al., 2012; Robert G. Loucks et al., 2012; Brian et al., 2013; Curtis et al., 2013; Jennings and Antia, 2013; Milliken et al., 2013; Schieber, 2013; Loucks and Reed, 2014; Pommer and Milliken, 2015) for varying shale systems to illustrate the occurrence of organic pores with increasing maturity.

Literature	Shale	Authors' Figure	R_o (%)	Organic Pore	Note
Curtis et al., 2013	Avalon	Figure 3	0.67	No	
Curtis et al., 2013	Avalon	Figure 4	0.75	Yes	Sponge-like
Chalmers et al., 2012	Doig	Figure 13	1.45	Yes	Sponge-like
Pommer &Milliken, 2015	Eagle Ford	Figure 2-A	0.5	No	
Pommer &Milliken, 2015	Eagle Ford	Figure 3-G	0.5	Yes	Primary-pore?
Pommer &Milliken, 2015	Eagle Ford	Figure 4	0.5	No	
Pommer &Milliken, 2015	Eagle Ford	Figure 5-A/C	0.5	No	
Jennings &Antia, 2013	Eagle Ford	Figure 6-A/B	<0.7	No	
Jennings &Antia, 2013	Eagle Ford	Figure 7-A	<0.7	No	
Loucks &Reed, 2014	Eagle Ford	Figure 3-D	0.75	Yes	Bubble-like
Loucks &Reed, 2014	Eagle Ford	Figure 4-C/D	0.8	Yes	Sponge-like
Loucks &Reed, 2014	Eagle Ford	Figure 5-D	0.8	Yes	Sponge-like
Driskill et al., 2013	Eagle Ford	Figure 13	0.77-0.82	Yes	Isolated
Driskill et al., 2013	Eagle Ford	Figure 14	0.77-0.82	Yes	Bubble-like
Driskill et al., 2013	Eagle Ford	Figure 15	0.79-0.86	Yes	Bubble-like
Jennings &Antia, 2013	Eagle Ford	Figure 7-B	0.7-1.0	Yes	Bubble-like
Jennings &Antia, 2013	Eagle Ford	Figure 6-C/D	>1.0	Yes	Sponge-like
Driskill et al., 2013	Eagle Ford	Figure 16	1.25	Yes	Bubble&Sponge
Driskill et al., 2013	Eagle Ford	Figure 27	1.25	Yes	Bubble&Sponge
Pommer &Milliken, 2015	Eagle Ford	Figure 2-C	1.3	Yes	Bubble&Sponge
Pommer &Milliken, 2015	Eagle Ford	Figure 3-H	1.3	Yes	Bubble&Sponge
Pommer &Milliken, 2015	Eagle Ford	Figure 6-C/D/F	1.3	Yes	Bubble&Sponge
Pommer &Milliken, 2015	Eagle Ford	Figure 14	1.3	Yes	Bubble&Sponge
Loucks &Reed, 2014	Eagle Ford	Figure 6-B	1.4	Yes	Aligned-kerogen
Loucks &Reed, 2014	Eagle Ford	Figure 6-A	1.5	Yes	Sponge-like
Jennings &Antia, 2013	Eagle Ford	Figure 7-C/D/E/F/G	1.4-1.6	Yes	Bubble&Sponge
Driskill et al., 2013	Eagle Ford	Figure 18	1.42-1.68	Yes	Bubble&Sponge
Jennings &Antia, 2013	Eagle Ford	Figure 7-H	1.6-1.8	Yes	Bubble-like
Schieber et al., 2010	Geneseo	Figure 6-C/D/E	>1.5	Yes	Sponge-like
Milner et al., 2010	Haynesville	Figure 4-A/B	1.8	Yes	Sponge-like
Chalmers et al., 2012	Haynesville	Figure 7	2.37	Yes	Sponge-like
Loucks et al., 2012	J-Bossier	Figure 13-B	1.24	Yes	Isolated
Curtis et al., 2012	Woodford	Figure 4	0.51	No	
Curtis et al., 2012	Woodford	Figure 4	0.76	No	
Curtis et al., 2012	Woodford	Figure 3-A	0.9	No	
Curtis et al., 2012	Woodford	Figure 4	0.90	No	
Curtis et al., 2012	Woodford	Figure 4	1.23	Yes	Sponge-like
Curtis et al., 2012	Woodford	Figure 6	1.4	Yes	Sponge-like
Chalmers et al., 2012	Woodford	Figure 9	1.51	Yes	Sponge-like
Curtis et al., 2012	Woodford	Figure 3-B	1.67	Yes	Sponge-like
Curtis et al., 2012	Woodford	Figure 4	1.67	Yes	Bubble&Sponge
Curtis et al., 2012	Woodford	Figure 4	2	No	Maceral difference?
Curtis et al., 2012	Woodford	Figure 4	3.60	Yes	Bubble-like
Curtis et al., 2012	Woodford	Figure 4	6.36	Yes	Isolated

Table 4. Continued (Milner et al., 2010; Schieber, 2010; Curtis et al., 2011; Curtis et al., 2012; Gareth R. Chalmers et al., 2012; Robert G. Loucks et al., 2012; Brian et al., 2013; Curtis et al., 2013; Jennings and Antia, 2013; Milliken et al., 2013; Schieber, 2013; Loucks and Reed, 2014; Pommer and Milliken, 2015)

Literature	Shale	Authors' Figure	R_o (%)	Organic Pore	Note
Milliken et al., 2013	Marcellus	Figure 4	1	Yes	Isolated
Milner et al., 2010	Marcellus	Figure 5-C/D	1.05	Yes	Bubble-like
Curtis et al., 2011	Marcellus	Figure 2	>1.1	Yes	Sponge-like
Chalmers et al., 2012	Marcellus	Figure 10	1.56	Yes	Bubble&Sponge
Milliken et al., 2013	Marcellus	Figure 6-D	2.1	Yes	Sponge-like
Milliken et al., 2013	Marcellus	Figure 7-C/D	2.1	Yes	Woody&Sponge
Milliken et al., 2013	Marcellus	Figure 8-A	2.1	Yes	Woody&Sponge
Schieber, 2013	Marcellus	Figure 12-C/D/E/F	2.1	Yes	Bubble&Sponge
Curtis et al., 2011	Marcellus	Figure 3	>3.1	Yes	Sponge-like
Loucks et al., 2012	New Albany	Figure 6-F	0.5	No	
Loucks et al., 2012	New Albany	Figure 9-F	0.5	No	
Schieber et al., 2010	New Albany	Figure 6-A/B	~0.5	No	
Schieber, 2013	New Albany	Figure 4-B	0.57	No	
Schieber, 2013	New Albany	Figure 6	0.57	No	
Schieber, 2013	New Albany	Figure 8	0.57	No	
Loucks et al., 2012	Pearsall	Figure 11-F	0.78	Yes	Desiccation-pore?
Loucks &Reed, 2014	Pearsall	Figure 6-C	0.78	Yes	Devolatilization-crack
Loucks &Reed, 2014	Pearsall	Figure 6-D	0.78	Yes	Desiccation-pore?
Loucks &Reed, 2014	Pearsall	Figure 4-A	1.2	No	Devolatilization-crack
Loucks et al., 2012	Pearsall	Figure 6-A	1.5	Yes	Isolated
Loucks et al., 2012	Pearsall	Figure 7-D	1.5	Yes	Bubble-like
Loucks et al., 2012	Pearsall	Figure 8-A	1.5	Yes	Sponge-like
Loucks et al., 2012	Pearsall	Figure 8-F	1.5	Yes	Bubble-like
Loucks et al., 2012	Pearsall	Figure 10-C	1.5	Yes	Bubble-like
Loucks et al., 2012	Pearsall	Figure 10-D	1.5	Yes	Bubble-like
Loucks et al., 2012	Pearsall	Figure 13-C	1.5	Yes	Isolated
Loucks et al., 2012	Pearsall	Figure 11-D	1.8	Yes	Sponge-like

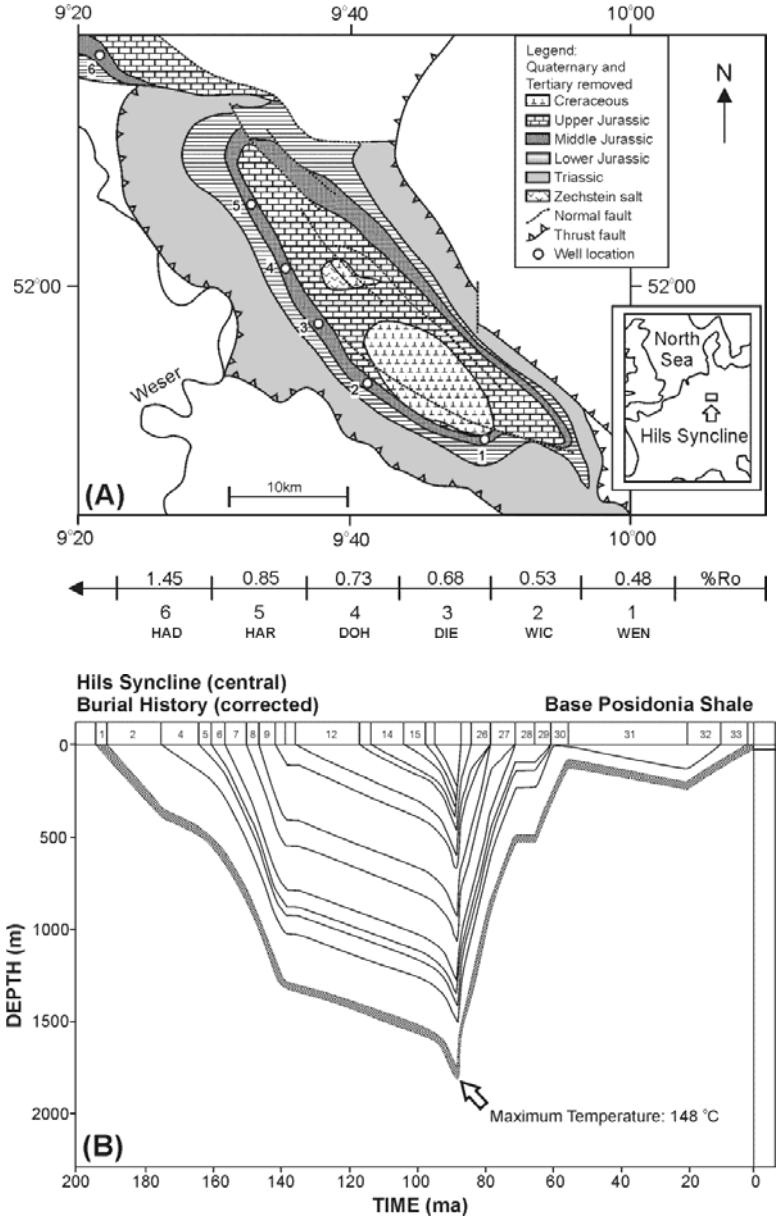

Figure 1. (A) The locations of studied six Posidonia wells, namely Wenzen (WEN), Wickensen (WIC), Dielmissen (DIE), Dohnsen (DOH), Harerode (HAR) and Haddessen (HAD), in the Hils Syncline area, after Horsfield et al. (1998). (B) The burial history of Posidonia Shale at the Harderode site, after Düppenbecker (1992).

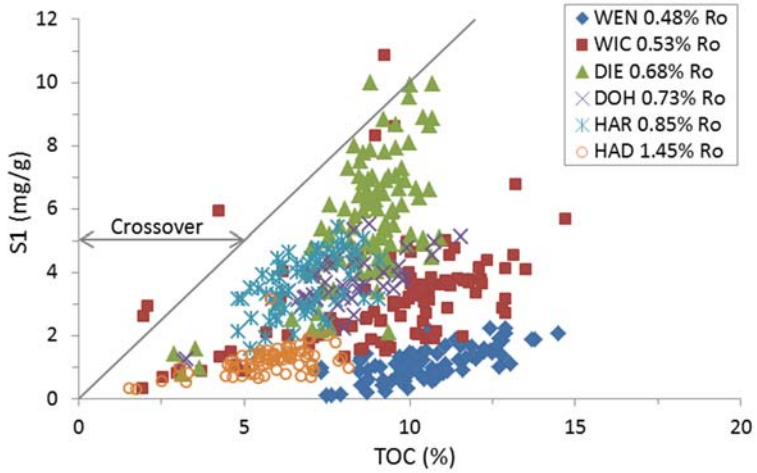

Figure 2. S1 versus TOC in six wells of the Posidonia Shale. Wells are ranked in the order of increasing maturity (measured vitrinite reflectance, %R_o) in the legend.

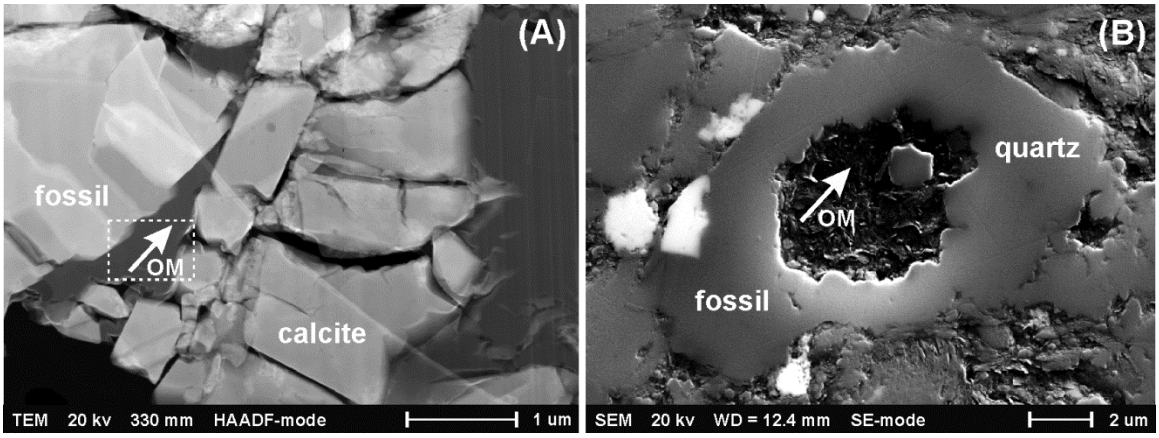

Figure 3. Organic matter (OM) filling pores of fossil associated. (A) TEM image (HAADF, Z-contrast mode) of a focused ion beam (FIB) foil extracted from the Wickensen well of Posidonia Shale. Dashed rectangle marked area is magnified in Figure 9A. (B) SEM image (secondary electron [SE] mode) of a thin section from the Marathon 1 Mesquite well, Barnett Shale. Organic matter (OM) filling in the chamber of sponge spicule is possibly bitumen.

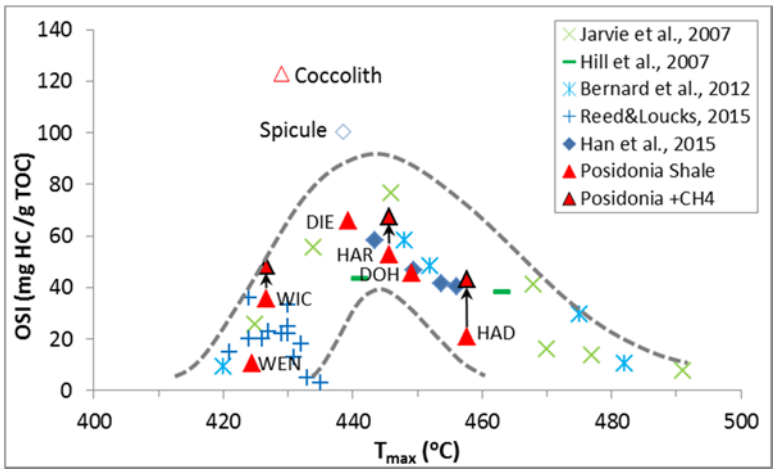

Figure 4. Retention capacity (OSI) as function of T_{max} in the Posidonia and Barnett shales. OSI = oil saturation index (S1/TOC × 100), S1 corresponds to the hydrocarbons volatilized at or below 300 °C in Rock-Eval analysis, and the TOC (total organic carbon) is measured by the Leco method. Modified OSI values by adding the maximum amounts of excess sorbed methane are marked by black arrows.

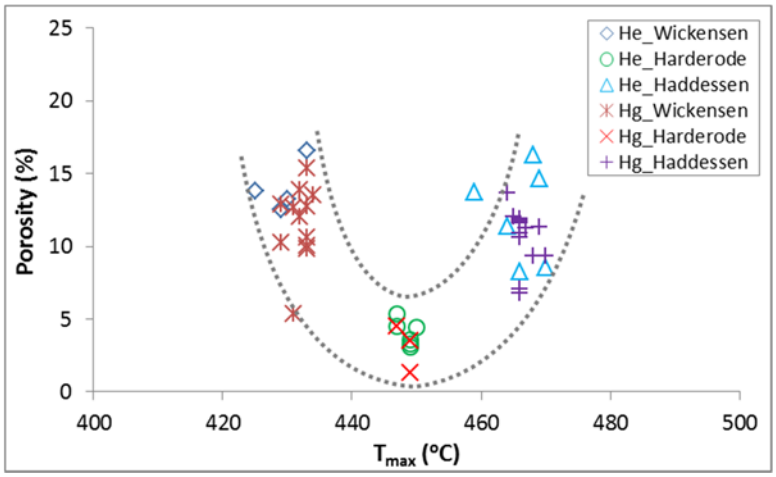

Figure 5. Porosity evolves with increasing maturity (T_{max}) in the Posidonia Shale. T_{max} corresponds to the temperature at which hydrocarbon generation rate is maximal during pyrolysis. Porosity is measured by mercury (Hg) injection porosimetry and helium (He) pycnometry techniques.

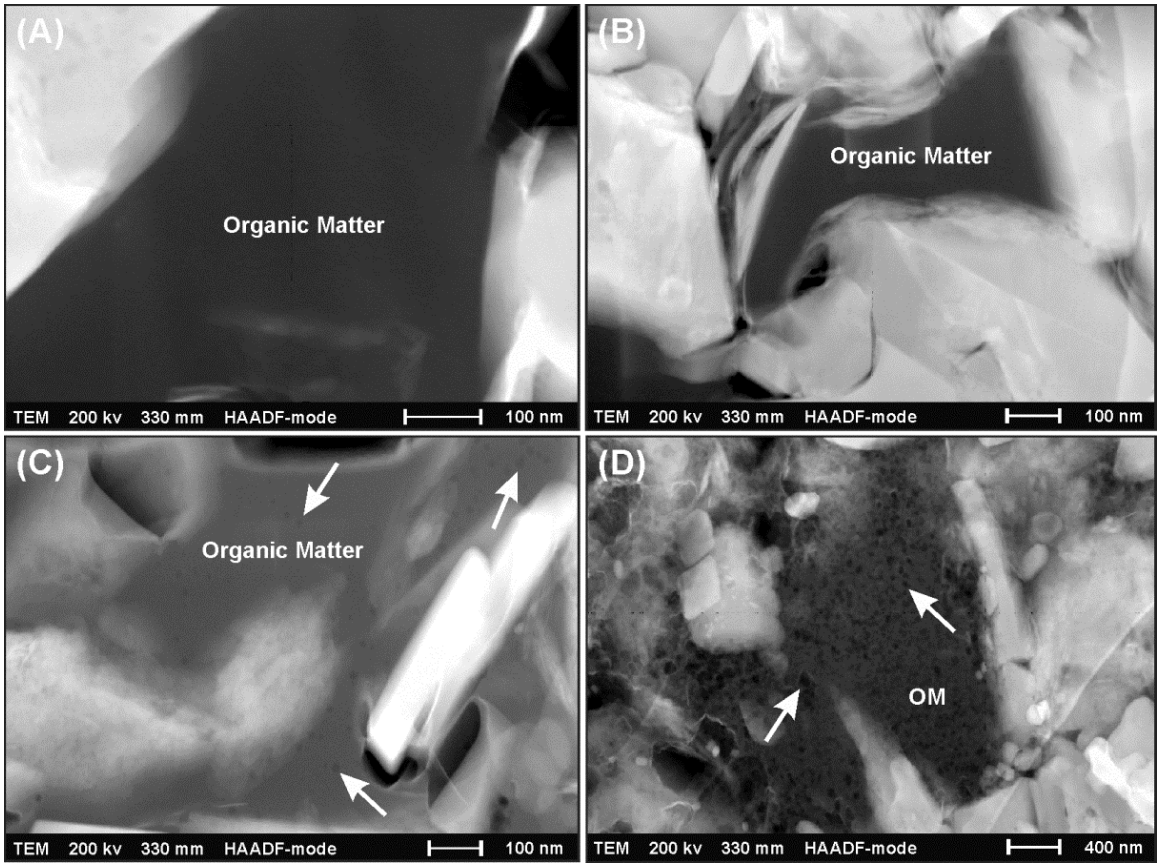

Figure 6. TEM images (HAADF mode, Z-contrast) of FIB foils extracted from Posidonia Shale samples of increasing maturity (T_{max}). (A) Wickensen well (427 ºC T_{max}), no TEM visible (~2 nm) organic pores. (B) Harderode well (446 ºC T_{max}), no pores developed within the organic matter. (C) Dohnsen well (449 ºC T_{max}), isolated bubble-like nanopores are scattered within the organic matter. (D) Haddessen well (458 ºC T_{max}), OM-hosted nanopores with spongy appearance of the organic matter (OM).

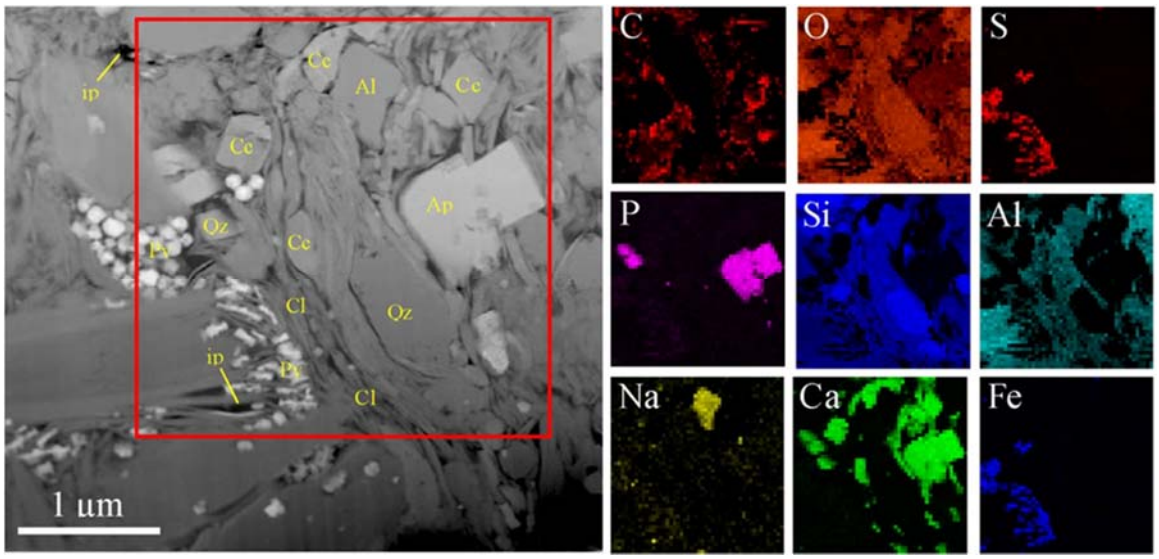

Figure 7. Left, TEM image (HAADF, Z-contrast mode) of a FIB foil from the Harderode well. Pores appear black, organic matter appears dark, silicates and carbonates appear grey, pyrite appears white. Square denotes area of energy-dispersive X-ray spectroscopy (EDXS) elemental maps (right): carbon (C), oxygen (O), sulphur (S), phosphorus (P), silicon (Si), aluminium (Al), sodium (Na), calcium (Ca) and iron (Fe). Authigenic pyrite (Py), calcium carbonates (Cc), apatite (Ap) and quartz (Qz) cements are identified. A few interparticular pores (ip) can be observed.

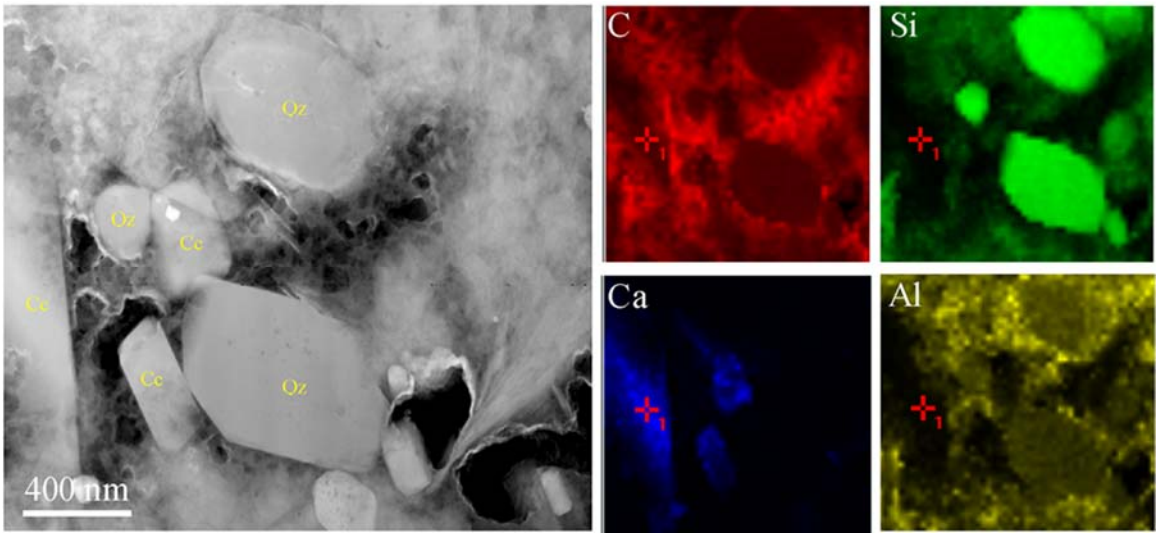

Figure 8. Left, TEM image (HAADF, Z-contrast mode) of a FIB foil from the Haddessen well. Pores appear black, organic matter appears dark, silicates and carbonates appear grey. Right, energy-dispersive X-ray spectroscopy (EDXS) elemental maps: carbon (C), silicon (Si), calcium (Ca) and aluminium (Al). Authigenic calcium carbonates (Cc) and quartz (Qz) cements are identified. The organic nanopores exhibit irregular shapes. The observed organic matter is extremely porous (>50 vol.%), possibly of bitumen origin. If this is the case, the former pore spaces are reclaimed by secondary cracking.

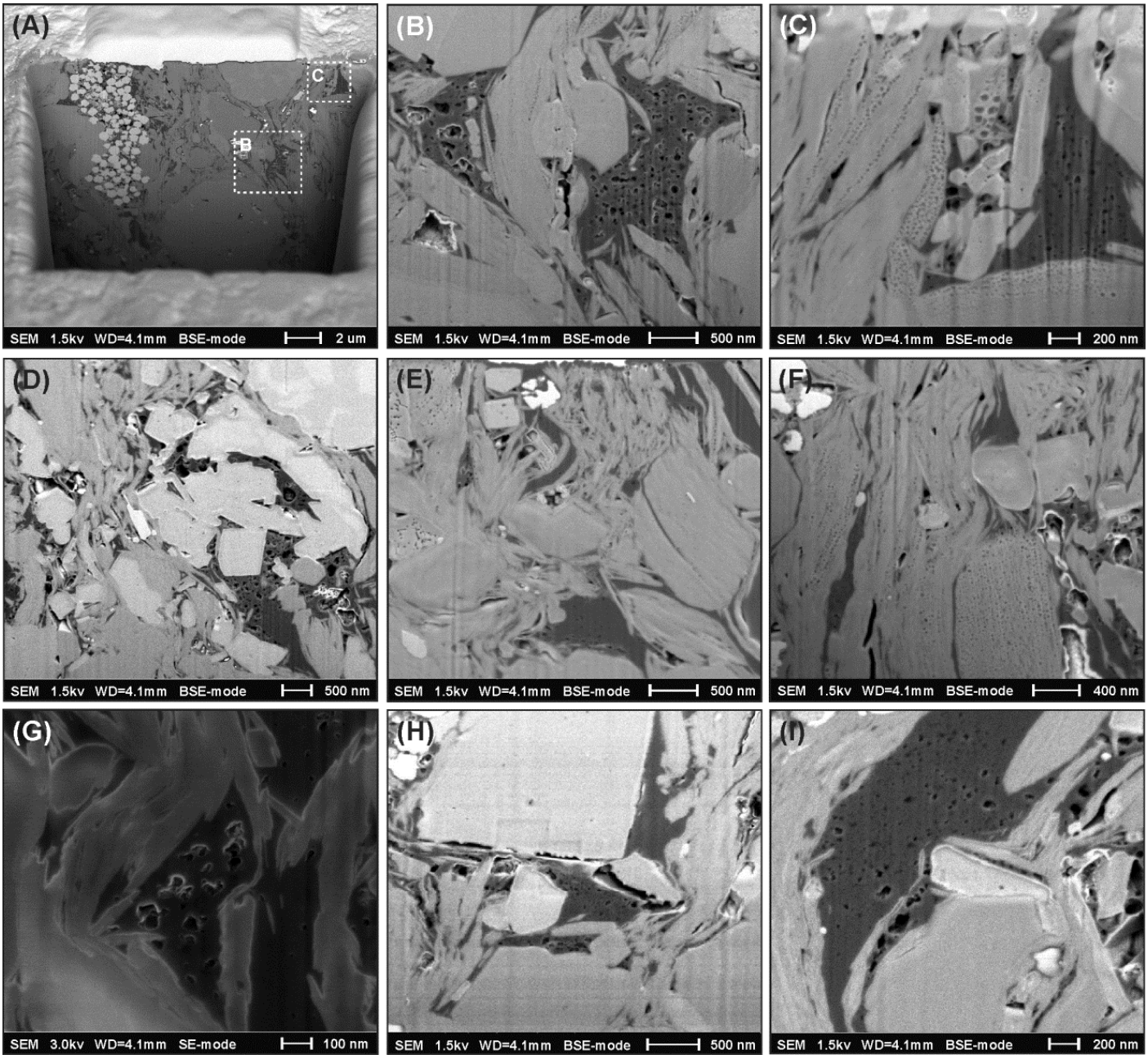

Figure 9. Scanning electron microscopy (SEM) images (back scattered electron [BSE] mode and secondary electron [SE] mode) of FIB milled trenches from the gas-mature Haddessen well (458 ºC T_{max}, 1.45% R_o), OM-hosted nanopores show significant heterogeneity amongst different kerogen particles. Dashed rectangle marked areas of Figure 8A are magnified in Figure 8B and Figure 8C, respectively.

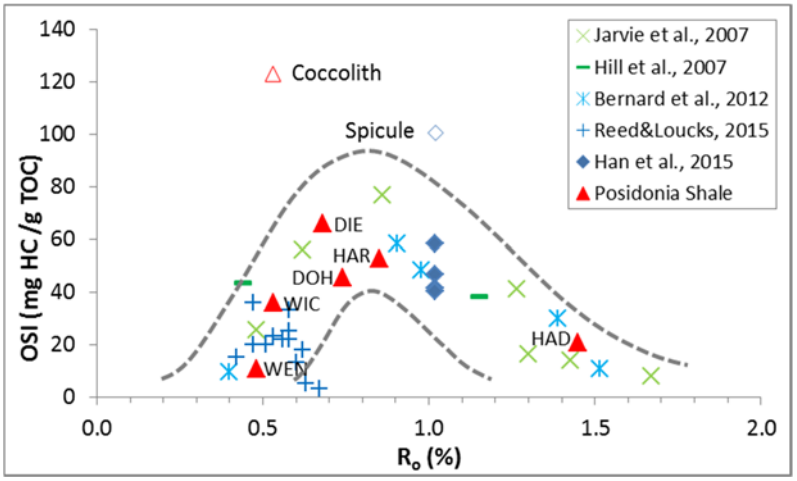

Figure 10. Retention capacity as function of maturity (R_o) in the Posidonia and Barnett shales. Vitrinite reflectance values of Posidonia Shale are taken from Rullkötter and Marzi (1988). Some vitrinite reflectance of Barnett Shale were converted from T_{max} values by applying the equation: R_o (%) = 0.018 × T_{max} – 7.16 (Jarvie et al., 2007).

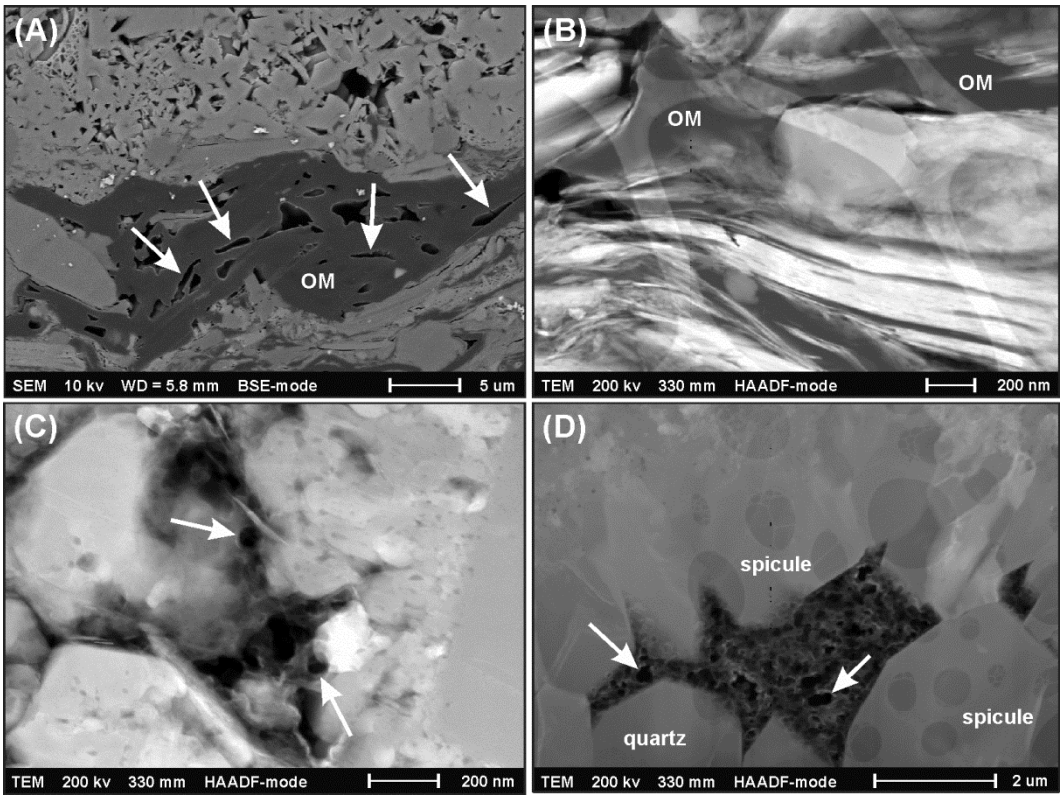

Figure 11. SEM image (back scattered electron [BSE] mode) of a FIB foil extracted from the immature Posidonia Shale (Figure 11A), and TEM images (HAADF, Z-contrast mode) of FIB foils extracted from the Barnett Shale (Figure 11B-D). (A) Elongated organic pores of primary origin. (B) Compaction features associated with clay minerals, no TEM visible (~2nm) organic pores. (C) Organic pores of possibly bitumen origin. (D) Organic pores of possible bitumen origin in the chamber of sponge spicule.

REFERENCES

Baker, D. R., 1962, Organic geochemistry of Cherokee Group in southeastern Kansas and northeastern Oklahoma: AAPG Bulletin, v. 46, no. 9, p. 1621-1642.

Baskin, D. K., and K. E. Peters, 1992a, Early generation characteristics of a sulfur-rich Monterey kerogen: AAPG Bull., v. 76, no. 1, p. 1-13.

Baskin, D. K., and K. E. Peters, 1992b, Early generation characteristics of a sulfur-rich Monterey kerogen: AAPG Bulletin, v. 76, no. 1, p. 1-13.

Behar, F., and M. D. Jarvie, 2013, Compositional Modeling of Gas Generation from Two Shale Gas Resource Systems: Barnett Shale (United States) and Posidonia Shale (Germany), *in* J.-Y. Chatellier, and D. M. Jarvie, eds., AAPG Memoir 103, American Association of Petroleum Geologists, p. 25-44.

Bernard, S., B. Horsfield, H.-M. Schulz, R. Wirth, A. Schreiber, and N. Sherwood, 2012a, Geochemical evolution of organic-rich shales with increasing maturity: A STXM and TEM study of the Posidonia Shale (Lower Toarcian, northern Germany): Marine and Petroleum Geology, v. 31, no. 1, p. 70-89, doi:10.1016/j.marpetgeo.2011.05.010.

Bernard, S., R. Wirth, A. Schreiber, H.-M. Schulz, and B. Horsfield, 2012b, Formation of nanoporous pyrobitumen residues during maturation of the Barnett Shale (Fort Worth Basin): International Journal of Coal Geology, v. 103, no. 0, p. 3-11, doi:10.1016/j.coal.2012.04.010.

Bernard, S., R. Wirth, A. Schreiber, L. Bowen, A. Aplin, E. Mathia, H.-M. Schulz, and B. Horsfield, 2013, FIB-SEM and TEM Investigations of an Organic-rich Shale Maturation Series from the Lower Toarcian Posidonia Shale, Germany: Nanoscale Pore System and Fluid-rock Interactions, *in* W. Camp, E. Diaz, and B. Wawak, eds., AAPG Memoir 102, American Association of Petroleum Geologists, p. 53-66.

Bowker, K. A., 2003, Recent development of the Barnett Shale play, Fort Worth basin: West Texas Geological Society Bulletin, v. 42, no. 6, p. 4-11.

Brian, D., W. Joel, D. Juliana, and W. S. Steven, 2013, Applications of SEM Imaging to Reservoir Characterization in the Eagle Ford Shale, South Texas, U.S.A, *in* W. Camp, E. Diaz, and B. Wawak, eds., AAPG Memoir 102, American Association of Petroleum Geologists, p. 115-136.

Cooles, G. P., A. S. Mackenzie, and T. M. Quigley, 1986, Calculation of petroleum masses generated and expelled from source rocks: Organic Geochemistry, v. 10, no. 1–3, p. 235-245, doi:10.1016/0146-6380(86)90026-4.

Curtis, M. E., R. J. Ambrose, C. H. Sondergeld, and C. S. Rai, 2011, Investigation of the Relationship Between Organic Porosity and Thermal Maturity in The Marcellus Shale, SPE North American Unconventional Gas Conference and Exhibition, Woodlands, Texas, USA, Society of Petroleum Engineers.

Curtis, M. E., B. J. Cardott, C. H. Sondergeld, and C. S. Rai, 2012, Development of organic porosity in the Woodford Shale with increasing thermal maturity: International Journal of Coal Geology, v. 103, p. 26-31, doi:10.1016/j.coal.2012.08.004.

Curtis, M. E., C. H. Sondergeld, and C. S. Rai, 2013, Relationship Between Organic Shale Microstructure and Hydrocarbon Generation, Unconventional Resources Conference-USA, Woodlands, Texas, USA, Society of Petroleum Engineers.

Dieckmann, V., H. J. Schenk, B. Horsfield, and D. H. Welte, 1998, Kinetics of petroleum generation and cracking by programmed-temperature closed-system pyrolysis of Toarcian Shales: Fuel, v. 77, no. 1–2, p. 23-31, doi:10.1016/S0016-2361(97)00165-8.

Düppenbecker, S. J., 1992, Genese und Expulsion von Kohlenwasserstoffen in zwei Regionen des Niedersächsischen Beckens unter besonderer Berücksichtigung der Aufheizraten, RWTH Aachen University, 304 p.

Ertas, D., S. R. Kelemen, and T. C. Halsey, 2006, Petroleum expulsion part 1. Theory of kerogen swelling in multicomponent solvents: Energy & Fuels, v. 20, no. 1, p. 295-300, doi:10.1021/ef058024k.

Espitalie, J., M. Madec, B. Tissot, J. J. Mennig, and P. Leplat, 1977, Source rock characterization method for petroleum exploration, Offshore Technology Conference, Houston, Texas, USA, Offshore Technology Conference, p. 439-444.

Gareth R. Chalmers, R. Marc Bustin, and I. M. Power, 2012, Characterization of gas shale pore systems by porosimetry, pycnometry, surface area, and field emission scanning electron microscopy/transmission electron microscopy image analyses: Examples from the Barnett, Woodford, Haynesville, Marcellus, and Doig units: AAPG Bulletin, v. 96, no. 6, p. 1099-1119, doi:10.1306/10171111052.

Gasparik, M., A. Ghanizadeh, P. Bertier, Y. Gensterblum, S. Bouw, and B. M. Krooss, 2012, High-Pressure Methane Sorption Isotherms of Black Shales from The Netherlands: Energy & Fuels, v. 26, no. 8, p. 4995-5004, doi:10.1021/ef300405g.

Gasparik, M., P. Bertier, Y. Gensterblum, A. Ghanizadeh, B. M. Krooss, and R. Littke, 2014, Geological controls on the methane storage capacity in organic-rich shales: International Journal of Coal Geology, v. 123, no. 0, p. 34-51, doi:10.1016/j.coal.2013.06.010.

Han, Y., N. Mahlstedt, and B. Horsfield, 2015, The Barnett Shale: compositional fractionation associated with intraformational petroleum migration, retention and expulsion: AAPG Bulletin, v. 99, no. 12, p. 2173-2202, doi:10.1306/06231514113.

Hedberg, H. D., 1936, Gravitational compaction of clays and shales: American Journal of Science, v. 31, no. 184, p. 241-287, doi:10.2475/ajs.s5-31.184.241.

Hill, R. J., E. Zhang, B. J. Katz, and Y. Tang, 2007a, Modeling of gas generation from the Barnett Shale, Fort Worth Basin, Texas: AAPG Bulletin, v. 91, no. 4, p. 501-521, doi:10.1306/12060606063.

Hill, R. J., D. M. Jarvie, J. Zumberge, M. Henry, and R. M. Pollastro, 2007b, Oil and gas geochemistry and petroleum systems of the Fort Worth Basin: AAPG Bulletin, v. 91, no. 4, p. 445-473, doi:10.1306/11030606014.

Horsfield, B., 1989, Practical criteria for classifying kerogens: Some observations from pyrolysis-gas chromatography: Geochimica et Cosmochimica Acta, v. 53, no. 4, p. 891-901, doi:10.1016/0016-7037(89)90033-1.

Horsfield, B., H. Clegg, H. Wilkes, and D. Santamaría-Orozco, 1998, Effect of maturity on carbazole distributions in petroleum systems: new insights from the Sonda de Campeche, Mexico, and Hils Syncline, Germany: Naturwissenschaften, v. 85, no. 5, p. 233-237, doi:10.1007/s001140050489.

Jarvie, D. M., R. J. Hill, and R. M. Pollastro, 2005, Assessment of the gas potential and yields from shales: the Barnett Shale model, *in* C. B.J., ed., Unconventional Energy Resources in the Southern Midcontinent, Oklahoma, USA, Oklahoma Geological Survey, p. 37-50.

Jarvie, D. M., R. J. Hill, T. E. Ruble, and R. M. Pollastro, 2007, Unconventional shale-gas systems: The Mississippian Barnett Shale of north-central Texas as one model for thermogenic shale-gas assessment: AAPG Bulletin, v. 91, no. 4, p. 475-499, doi:10.1306/12190606068.

Jarvie, D. M., 2012, Shale resource systems for oil and gas: Part 2 —Shale-oil resource systems, *in* J. A. Breye, ed., AAPG Memoir 97, American Association of Petroleum Geologists, p. 89-119.

Jennings, D. S., and J. Antia, 2013, Petrographic Characterization of the Eagle Ford Shale, South Texas, Mineralogy, Common Constituents, and Distribution of Nanometer-scale Pore Types, *in* W. Camp, E. Diaz, and B. Wawak, eds., AAPG Memoir 102, American Association of Petroleum Geologists, p. 101-113.

Jochum, J., G. Friedrich, D. Leythaeuser, R. Littke, and B. Ropertz, 1995, Hydrocarbon-bearing fluid inclusions in calcite-filled horizontal fractures from mature Posidonia Shale (Hils Syncline, NW Germany): Ore Geology Reviews, v. 9, no. 5, p. 363-370, doi:10.1016/0169-1368(94)00019-K.

Kelemen, S. R., C. C. Walters, D. Ertas, H. Freund, and D. J. Curry, 2006a, Petroleum expulsion part 3. A model of chemically driven fractionation during expulsion of petroleum from kerogen: Energy & Fuels, v. 20, no. 1, p. 309-319, doi:10.1021/ef058023s.

Kelemen, S. R., C. C. Walters, D. Ertas, L. M. Kwiatek, and D. J. Curry, 2006b, Petroleum expulsion part 2. Organic matter type and maturity effects on kerogen swelling by solvents and thermodynamic parameters for kerogen from regular solution theory: Energy & Fuels, v. 20, no. 1, p. 301-308, doi:10.1021/ef0580220.

Larsen, J. W., and S. Li, 1997, Changes in the macromolecular structure of a type I kerogen during maturation: Energy & Fuels, v. 11, no. 4, p. 897-901, doi:10.1021/ef970007a.

Larter, S., 1988, Some pragmatic perspectives in source rock geochemistry: Marine and Petroleum Geology, v. 5, no. 3, p. 194-204, doi:10.1016/0264-8172(88)90001-3.

Littke, R., D. R. Baker, and D. Leythaeuser, 1988, Microscopic and sedimentologic evidence for the generation and migration of hydrocarbons in Toarcian source rocks of different maturities: Organic Geochemistry, v. 13, no. 1–3, p. 549-559, doi:10.1016/0146-6380(88)90075-7.

Löhr, S. C., E. T. Baruch, P. A. Hall, and M. J. Kennedy, 2015, Is organic pore development in gas shales influenced by the primary porosity and structure of thermally immature organic matter?: Organic Geochemistry, v. 87, p. 119-132, doi:10.1016/j.orggeochem.2015.07.010.

Lopatin, N. V., S. L. Zubairaev, I. M. Kos, T. P. Emets, E. A. Romanov, and O. V. Malchikhina, 2003, Uncoventional oil accumulations in the Upper Jurassic Bazhenov Black Shale Formation, West Siberian Basin: A self-sourced reservoir system: Journal of Petroleum Geology, v. 26, no. 2, p. 225-244, doi:10.1111/j.1747-5457.2003.tb00027.x.

Loucks, R. G., and S. C. Ruppel, 2007, Mississippian Barnett Shale: Lithofacies and depositional setting of a deep-water shale-gas succession in the Fort Worth Basin, Texas: AAPG Bulletin, v. 91, no. 4, p. 579-601, doi:10.1306/11020606059.

Loucks, R. G., R. M. Reed, S. C. Ruppel, and D. M. Jarvie, 2009, Morphology, genesis, and distribution of nanometer-scale pores in siliceous mudstones of the Mississippian Barnett Shale: Journal of Sedimentary Research, v. 79, no. 12, p. 848-861.

Loucks, R. G., and R. M. Reed, 2014, Scanning-Electron-Microscope Petrographic Evidence for Distinguishing Organic-Matter Pores Associated with Depositional Organic Matter versus Migrated Organic Matter in Mudrocks: Gulf Coast Assoc. Geol. Soc., v. 3, p. 51-60.

Mastalerz, M., A. Schimmelmann, A. Drobniak, and Y. Chen, 2013, Porosity of Devonian and Mississippian New Albany Shale across a maturation gradient: Insights from organic petrology, gas adsorption, and mercury intrusion: AAPG Bulletin, v. 97, no. 10, p. 1621-1643, doi:10.1306/04011312194.

Milliken, K., S.-J. Choh, P. Papazis, and J. Schieber, 2007, "Cherty" stringers in the Barnett Shale are agglutinated foraminifera: Sedimentary Geology, v. 198, no. 3–4, p. 221-232, doi:10.1016/j.sedgeo.2006.12.012.

Milliken, K. L., M. Rudnicki, D. N. Awwiller, and T. Zhang, 2013, Organic matter–hosted pore system, Marcellus Formation (Devonian), Pennsylvania: AAPG Bulletin, v. 97, no. 2, p. 177-200, doi:10.1306/07231212048.

Milner, M., R. McLin, and J. Petriello, 2010, Imaging Texture and Porosity in Mudstones and Shales: Comparison of Secondary and Ion-Milled Backscatter SEM Methods, Canadian Unconventional Resources & International Petroleum Conference, Calgary, Alberta, Canada, Society of Petroleum Engineers.

Okiongbo, K. S., A. C. Aplin, and S. R. Larter, 2005, Changes in Type II Kerogen Density as a Function of Maturity: Evidence from the Kimmeridge Clay Formation: Energy & Fuels, v. 19, no. 6, p. 2495-2499, doi:10.1021/ef050194+.

Passey, Q. R., K. Bohacs, W. L. Esch, R. Klimentidis, and S. Sinha, 2010, From Oil-Prone Source Rock to Gas-Producing Shale Reservoir - Geologic and Petrophysical Characterization of Unconventional Shale Gas Reservoirs, CPS/SPE International Oil & Gas Conference and Exhibition, Beijing, China, Society of Petroleum Engineers.

Pepper, A. S., 1992, Estimating the petroleum expulsion behaviour of source rocks: a novel quantitative approach: Geological Society, London, Special Publications, v. 59, no. 1, p. 9-31, doi:10.1144/gsl.sp.1991.059.01.02.

Peters, K. E., 1986, Guidelines for evaluating petroleum source rock using programmed pyrolysis: AAPG Bulletin, v. 70, no. 3, p. 318-329.

Pollastro, R. M., 2010, Natural Fractures, Composition, Cyclicity, and Diagenesis of the Upper Cretaceous Niobrara Formation, Berthoud Field, Colorado: The Mountain Geologist, v. 47, no. 4, p. 135-149.

Pommer, M., and K. Milliken, 2015, Pore types and pore-size distributions across thermal maturity, Eagle Ford Formation, southern Texas: AAPG Bulletin, v. 99, no. 9, p. 1713-1744, doi:10.1306/03051514151.

Price, L. C., L. M. Wenger, T. Ging, and C. W. Blount, 1983, Solubility of crude oil in methane as a function of pressure and temperature: Organic Geochemistry, v. 4, no. 3–4, p. 201-221, doi:10.1016/0146-6380(83)90042-6.

Price, L. C., and C. E. Baker, 1985, Suppression of vitrinite reflectance in amorphous rich kerogen-a major unrecognized problem:

Journal of Petroleum Geology, v. 8, no. 1, p. 59-84, doi:10.1111/j.1747-5457.1985.tb00191.x.
Radke, M., 1988, Application of aromatic compounds as maturity indicators in source rocks and crude oils: Marine and Petroleum Geology, v. 5, no. 3, p. 224-236, doi:10.1016/0264-8172(88)90003-7.
Reed, R. M., R. G. Loucks, and S. C. Ruppel, 2014, Comment on "Formation of nanoporous pyrobitumen residues during maturation of the Barnett Shale (Fort Worth Basin)" by Bernard et al. (2012): Int. J. Coal Geol., v. 127, p. 111-113, doi:10.1016/j.coal.2013.11.012.
Reed, R. M., and R. G. Loucks, 2015, Low-Thermal-Maturity (<0.7% VR) Mudrock Pore Systems: Mississippian Barnett Shale, Southern Fort Worth Basin: Gulf Coast Association of Geological Societies, v. 4, p. 15-28.
Rexer, T. F., E. J. Mathia, A. C. Aplin, and K. M. Thomas, 2014, High-Pressure Methane Adsorption and Characterization of Pores in Posidonia Shales and Isolated Kerogens: Energy & Fuels, v. 28, no. 5, p. 2886-2901, doi:10.1021/ef402466m.
Robert G. Loucks, Robert M. Reed, Stephen C. Ruppel, and U. Hammes, 2012, Spectrum of pore types and networks in mudrocks and a descriptive classification for matrix-related mudrock pores: AAPG Bulletin, v. 96, no. 6, p. 1071-1098, doi:10.1306/08171111061.
Robl, T. L., D. N. Taulbee, L. S. Barron, and W. C. Jones, 1987, Petrologic chemistry of a Devonian type II kerogen: Energy & Fuels, v. 1, no. 6, p. 507-513, doi:10.1021/ef00006a009.
Röhl, H.-J., A. Schmid-Röhl, W. Oschmann, A. Frimmel, and L. Schwark, 2001, The Posidonia Shale (Lower Toarcian) of SW-Germany: an oxygen-depleted ecosystem controlled by sea level and palaeoclimate: Palaeogeography, Palaeoclimatology, Palaeoecology, v. 165, no. 1–2, p. 27-52, doi:10.1016/S0031-0182(00)00152-8.
Rullkötter, J., and R. Marzi, 1988, Natural and artificial maturation of biological markers in a Toarcian shale from northern Germany: Organic Geochemistry, v. 13, no. 4–6, p. 639-645, doi:10.1016/0146-6380(88)90084-8.
Sandvik, E. I., W. A. Young, and D. J. Curry, 1992, Expulsion from hydrocarbon sources: the role of organic absorption: Organic Geochemistry, v. 19, no. 1–3, p. 77-87, doi:10.1016/0146-6380(92)90028-V.
Schettler, P. D., Jr., and C. R. Parmely, 1991, Contributions to total storage capacity in Devonian shales, SPE Eastern Regional Meeting, Lexington, Kentucky, USA, Society of Petroleum Engineers, p. 77-88.
Schieber, J., 2010, Common Themes in the Formation and Preservation of Intrinsic Porosity in Shales and Mudstones - Illustrated with Examples Across the Phanerozoic, SPE Unconventional Gas Conference, Pittsburgh, Pennsylvania, USA, Society of Petroleum Engineers.
Schieber, J., 2013, SEM Observations on Ion-milled Samples of Devonian Black Shales from Indiana and New York: The Petrographic Context of Multiple Pore Types, *in* W. Camp, E. Diaz, and B. Wawak, eds., AAPG Memoir 102, American Association of Petroleum Geologists, p. 153-171.
Sclater, J. G., and P. A. F. Christie, 1980, Continental stretching: An explanation of the Post-Mid-Cretaceous subsidence of the central North Sea Basin: Journal of Geophysical Research: Solid Earth, v. 85, no. B7, p. 3711-3739, doi:10.1029/JB085iB07p03711.
Stainforth, J. G., and J. E. A. Reinders, 1990, Primary migration of hydrocarbons by diffusion through organic matter networks, and its effect on oil and gas generation: Organic Geochemistry, v. 16, no. 1–3, p. 61-74, doi:10.1016/0146-6380(90)90026-V.
Tissot, B. P., Y. Califet-Debyser, G. Deroo, and J. L. Oudin, 1971, Origin and evolution of hydrocarbons in early Toarcian shales, Paris Basin, France: AAPG Bulletin, v. 55, no. 12, p. 2177-2193.
Tissot, B. P., and D. H. Welte, 1984, Petroleum formation and occurrence: Verlag, Berlin, Heidelberg, New York, Tokyo, Springer, 699 p.
Tissot, B. P., R. Pelet, and P. Ungerer, 1987, Thermal History of Sedimentary Basins, Maturation Indices, and Kinetics of Oil and Gas Generation: AAPG Bulletin, v. 71, no. 12, p. 1445-1466.
Ungerer, P., E. Behar, and D. Discamps, 1983, Tentative calculation of the overall volume expansion of organic matter during hydrocarbon genesis from geochemistry data: Advances in Organic Geochemistry, p. 129-135.
Wang, F. P., R. M. Reed, J. A., and K. G., 2009, Pore Networks and Fluid Flow in Gas Shales, SPE Annual Technical Conference and Exhibition, New Orleans, Louisiana, USA, Society of Petroleum Engineers.
Wirth, R., 2009, Focused Ion Beam (FIB) combined with SEM and TEM: Advanced analytical tools for studies of chemical composition, microstructure and crystal structure in geomaterials on a nanometre scale: Chemical Geology, v. 261, no. 3–4, p. 217-229, doi:10.1016/j.chemgeo.2008.05.019.

APPENDIX

Here we clarify the equations used in the main text in detail, with input data taken mainly from Table 2:

$$[1.226(g/cm^3) - 1.096(g/cm^3) = 0.130\ g/cm^3] \qquad \textbf{Equation (1)}$$

where 1.226 and 1.096 is the density of kerogen (pore-free, g/cm^3) in the Wickensen and Harderode wells, respectively.

$$[0.130(g/cm^3)/1.226(g/cm^3)\times 10.41(wt.\%) = 1.10\ wt.\%] \qquad \textbf{Equation (2)}$$

where 0.130 is the difference in kerogen density (g/cm^3) from Formula (S1), 1.226 is the density of kerogen (g/cm^3) in the Wickensen well, and 10.41 is the TOC (wt.%) of Wickensen well. The result 1.10 wt.% represents the specific loss of TOC due to the decrease of kerogen density caused by swelling from the Wickensen well to the Harderode well.

$$[10.41(wt.\%) - 7.90(wt.\%) = 2.51\ wt.\%] \qquad \textbf{Equation (3)}$$

where 10.41 and 7.90 is the TOC (wt.%) of the Wickensen and Harderode wells, respectively.

[10(%)×2.903(g/cm^3)×1(cm^3)/2.445(g/cm^3)×1(cm^3)×10.41(wt.%)= 1.24 wt.%] **Equation (4)**

where 10 is an approximate volume of dilution minerals (%) in the Harderode well, 2.903 is the approximate density (g/cm^3) of those minerals, and 10(%)×2.903(g/cm^3)×1(cm^3) is therefore the increasing mass (g) due to the dilution of varies minerals in 1 cm^3 rock. In the Harderode well, the weight of 1 cm^3 shale is 2.445(g/cm^3)×1(cm^3). Thus, the dilution ratio for the whole rock is 10(%)×2.903(g/cm^3)×1(cm^3)/2.445(g/cm^3)×1(cm^3). By multiplying the TOC (10.41 wt.%) of Wickensen well (the assumed precursor of the Harderode well), the decrease of TOC due to dilution is then calculated. Notably, Equation (4) is just an approximation, since the density of dilution minerals should be higher than 2.903 (g/cm^3).

[7.34(vol.%)/20.84(vol.%)×100% = 35%] **Equation (5)**

where 7.34 is the calculated volume (vol.%) of secondary organic pores in the Haddessen well, 20.84 is the assumed volume (vol.%) of less mature organic matter (that of Harderode well). The result 35% is thus the relative porosity formed within organic particles in the Haddessen well.

[12.13(vol.%) – 4.05(vol.%) = 8.08 vol.%] **Equation (6)**

where 12.13 and 4.05 is the pore volume (vol.%) in the Haddessen and Harderode wells, respectively.

[19.73(vol.%) – 12.50(vol.%) = 7.23 vol.%] **Equation (7)**

where 19.73 and 12.50 is the recalculated kerogen volume (vol.%) of the Harderode and Haddessen wells, respectively.

AUTHORS

YUANJIA HAN ~ Section 3.2 Organic Geochemistry, German Research Centre for Geosciences (GFZ), Telegrafenberg, Potsdam 14473, Germany; yuanjia@gfz-potsdam.de

Yuanjia Han is currently a Ph.D. student at the German Research Centre for Geosciences under the auspices of the Technical University of Berlin. He gained his B.S. and M.S. degrees from China University of Geosciences in 2010 and 2012, respectively. His research interests focus on the mechanisms of hydrocarbon retention and migration in unconventional shale reservoirs.

BRIAN HORSFIELD ~ Section 3.2 Organic Geochemistry, German Research Centre for Geosciences (GFZ), Telegrafenberg, Potsdam 14473, Germany; horsf@gfz-potsdam.de

Brian Horsfield is a Full Professor of Organic Geochemistry and Hydrocarbon Systems at the Technical University of Berlin, Germany, as well as leader of Organic Geochemistry at the German Research Centre for Geosciences. He is a member of the German Academy of Science and Technology. He has more than 30 years of experience working with and for industry in upstream research and development. The evaluation of gas-in-place and producibility in unconventional hydrocarbon systems of the USA, South Africa, China, Australia and North Africa are key activities in service and research at the present time.

RICHARD WIRTH ~ Section 4.3 Chemistry and Physics of Earth Materials, German Research Centre for Geosciences (GFZ), Telegrafenberg, Potsdam 14473, Germany; wirth@gfz-potsdam.de

Richard Wirth is a senior research scientist and lab supervisor at the German Research Centre for Geosciences. He studied Mineralogy and Electron Microscopy and holds a diploma and Ph.D. from the University of Würzburg. His work is focused on the application of Advanced Electron Microscopy (TEM, FIB).

NICOLAJ MAHLSTEDT ~ Section 3.2 Organic Geochemistry, German Research Centre for Geosciences (GFZ), Telegrafenberg, Potsdam 14473, Germany; nicolaj.mahlstedt@gfz-potsdam.de

Nicolaj Mahlstedt is a Postdoc at the German Research Centre for Geosciences. He studied Applied Geosciences and holds a diploma and Ph.D. from the Technical University of Berlin. He conducted his Ph.D. within the GFZ-Industry-Partnership-Program investigating “High Temperature Methane” generation. His major scientific interests include petroleum system analysis, oil and gas retention processes, compositional kinetic modelling and the development of geochemical screening tools.

SYLVAIN BERNARD ~ IMPMC, Sorbonne Universités, CNRS UMR 7590, MNHN, UPMC, 61 rue Buffon, 75005 Paris, France ; sbernard@mnhn.fr

Sylvain Bernard is a mineralogist/geochemist who started to work on unconventional shale-gas hydrocarbon systems in 2009 as a postdoctoral fellow at the GFZ (Potsdam, Germany). He now continues investigating the geological cycle of organic carbon as a permanent CNRS researcher at the IMPMC (Paris, France), using an original combination of in situ spectro-microscopy techniques, including cutting edge synchrotron-based tools.